JOURNAL PRE-PROOF

This is an early version of the article, published prior to copyediting, typesetting, and editorial correction. The manuscript has been accepted for publication and is now available online to ensure early dissemination, author visibility, and citation tracking prior to the formal issue publication.

It has not undergone final language verification, formatting, or technical editing by the journal's editorial team. Content is subject to change in the final Version of Record.

To differentiate this version, it is marked as "PRE-PROOF PUBLICATION" and should be cited with the provided DOI. A visible watermark on each page indicates its preliminary status.

The final version will appear in a regular issue of *Engineering Transactions*, with final metadata, layout, and pagination.

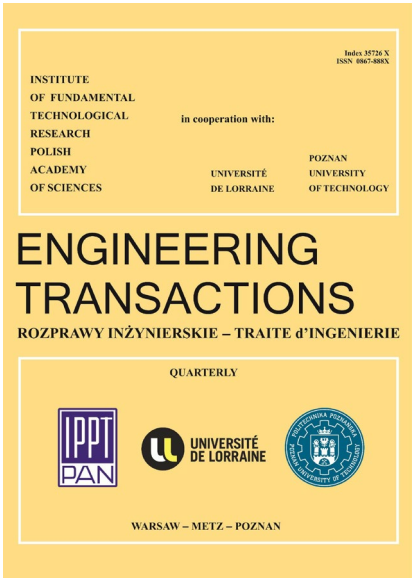

Title: Development of Online Monitoring Device for Ash Accumulation Status of Alkali Recovery Boiler

Author(s): Bo Wang, Caiming Zhang, Yuanli Wang

DOI: https://doi.org/10.24423/engtrans.2026.3559

Journal: *Engineering Transactions*

ISSN: 0867-888X, e-ISSN: 2450-8071

Publication status: In press

Received: 2025-04-24

Revised: 2025-07-28

Accepted: 2026-01-12

Published pre-proof: 2026-04-02

Please cite this article as:

Wang B., Zhang C., Wang Y., Development of Online Monitoring Device for Ash Accumulation Status of Alkali Recovery Boiler, *Engineering Transactions*, 2026, https://doi.org/10.24423/engtrans.2026.3559

Development of Online Monitoring Device for Ash Accumulation Status of Alkali Recovery Boiler

Bo WANG[1], Caiming ZHANG[1,*] Yuanli WANG[2]

[1] College of Mechanical and Electrical Engineering, Shaanxi University of Science and Technology, Xiaan, China

[2] China United Equipment Group Anyang Machinery Co., Ltd., Anyang, China

*Corresponding Author: 2293709175@qq.com

The alkali recovery boiler is an important piece of equipment in chemical pulp production. It uses papermaking black liquor as fuel. Due to the large number of impurities, the heating surface is prone to severe ash deposition. To improve the heat transfer coefficient, the traditional method is to carry out timed soot blowing, which has problems such as untimely ash cleaning or excessive steam consumption caused by overly frequent soot blowing. In this paper, an experimental device for the relationship between the heat transfer coefficient and the weight of ash deposition was developed. The functional relationship between the two was obtained. There is an inflection point when the amount of ash deposition reaches 294.77 g. A control strategy of soot blowing at the inflection point was further proposed. A load-strain experimental testing device was developed. Experiments show that when the weight of ash deposition reaches 3503 N, the deformation of the suspender is 9 με, and starting the soot blowing device is the most efficient when the heat transfer coefficient is 725.15 W/(m²·K). Therefore, the degree of decline of the heat transfer coefficient can be indirectly reflected by measuring the strain. A method of soot blowing by detecting the degree of suspender strain was further proposed. This method is more scientific than the original timed soot blowing method and provides a technical reference for the energy-saving and consumption-reduction theories and engineering applications of alkali recovery boilers.

Keywords: alkali recovery boiler; strain measurement; ash deposition detection; intelligent soot blowing; decline of heat transfer coefficient.

1. Introduction

In the papermaking industry, displacement cooking is mainly used in the pulping process. By heating to make water boil, the organic substances in the plant fiber raw materials are dissolved in the cooking alkali to form black liquor, which is then separated from the pulp. This provides a basis for subsequent black liquor treatment and alkali recovery[1]. The alkali recovery boiler uses the black liquor discharged after washing the pulp in the alkaline pulping process as fuel for combustion[2]. The concentrated black liquor is fed into the furnace for combustion to generate steam and melt. The steam can be reused as a secondary energy source, and the melt is causticized to be reduced to alkali for reuse in pulp cooking [3]. The alkali recovery boiler not only treats the waste liquid generated in the papermaking process but also realizes the recycling

of resources, energy conservation, and emission reduction[4]. However, during the combustion of black liquor, inorganic substances are vaporized at high temperatures and solidify in the flue gas in the furnace, forming ash deposits in the alkali recovery boiler[5]. In black liquor, silicon mainly exists in the form of sodium silicate. Sodium silicate is prone to form silicate at high temperatures, increasing the viscosity and hardness of the ash deposits, thus exacerbating the formation and blockage problems of ash deposits. Therefore, monitoring the degree of ash deposition on the heating surface of the boiler[6]and carrying out timely soot blowing play a very important role.

As early as the 1970s, research on on-line monitoring systems for boilers began one after another. For example, the Electric Power Research Institute of the United States focused its research on boiler fouling monitoring[7] and regarded the optimization of the boiler soot blowing mode as the key to improving the operation of boiler units[8]. The University of Waterloo placed a disk-type heat flux meter [9] to directly monitor the dynamic changes of the radiation in the furnace, and successfully developed a monitoring system[10] based on this. Scholars such as LeVert upgraded the heat flux meter [11]and introduced the pulse heater technology. The signal response time can directly reflect the real-time dynamics of the fouling in the furnace. Through the heat balance method [12], the whole process of pollution monitoring of the convective heating surface was realized. However, due to the complexity of the alkali recovery boiler, especially the intricate heat transfer processes of each heating surface[13], in this mechanism-based modeling method, a large number of simplifications have to be made to the actual process during the modeling process. Although this simplification reduces the complexity of modeling to a certain extent, it also significantly reduces the accuracy of the model. Especially when the boiler undergoes significant load changes, the impact of this simplification is more prominent, making it difficult for the model to accurately and reliably reflect the fouling conditions of the heating surface[14]. Scholar Pang Liping [15] simulated the operation processes of convective heat transfer and radiation based on the software developed by a Canadian simulation company. Scholars such as Ye Jiangming [16] completed the dynamic monitoring of ash deposition on the heating surface with the help of the Kriging model and the monitoring data collected from power plants. When studying the unit, scholars such as Zhang Hailin[17] found that the structure of the tail heating surface was extremely complex. They described it through the renormalization group and compared it with the random impedance network to obtain the thermal percolation model. This data algorithm-based modeling method relies on a large amount of data for analysis and training. On specific datasets, such methods can demonstrate excellent fouling monitoring effects. However, due to their dependence on and limitations of data, their generalization ability is relatively weak. That is, when facing different data distributions or complex and changeable actual situations, their monitoring effects may be greatly affected. In addition to using the heat flux meter method to monitor the fouling of the heating surface, some scholars have combined the heat transfer characteristics of the furnace and used other parameters to reflect the pollution state of the water wall, and achieved phased results. Scholars such as Wang Binzhong[18] built a model to judge the slagging degree in the furnace. This model is mainly realized through the temperature at the fin end on the back-fire side, opening up a new direction for judging the slagging situation in the furnace. It can be seen that for the research on the ash deposition monitoring and soot blowing control system of power plant boilers, the cleanliness coefficient of each heating surface is determined based on the heat

balance principle, and the severity of ash deposition on the boiler heating surface is reflected through index factors. This method is applicable to boilers with a single raw material and basically unchanged operating conditions[19]. Moreover, since the boiler is a complex system with multiple variables and strong coupling, and has a very large thermal inertia, the calculated cleanliness coefficient is not very accurate and it is difficult to guide real industrial production.

The soot blowing system [20] is one of the important systems of the alkali recovery boiler. Its main function is to blow the ash deposits on the heating surfaces such as the economizer, boiler tubes, and superheater of the alkali recovery furnace, so as to prevent a decrease in the thermal efficiency of the alkali furnace due to excessive ash deposition on the heating surfaces, and avoid situations such as forced shutdown for water washing caused by flue blockages [21].At present, the boiler soot blowing system mainly blows the ash on all heating surfaces at fixed time intervals. It is difficult to carry out soot blowing according to the actual ash deposition situation. Infrequent soot blowing will reduce the heat transfer efficiency of the boiler and degrade its performance. While frequent soot blowing [22] not only causes waste of high-pressure steam, but also wears the surface of the heating surface pipes, generates huge thermal stress, shortens the service life of the heat exchange device, and increases the maintenance cost of the soot blowers. The abnormal ash deposition and slagging attached to the heating surfaces in the furnace will have a direct impact on the operation of the boiler. For example, it will increase the heat transfer resistance and the ventilation resistance in the flue, cause the exhaust gas temperature of the unit to rise, reduce the thermal efficiency of the boiler, cause high-temperature corrosion, and shorten the actual service life of the equipment[23]. At the same time, the periodic collapse of loose ash deposits can also cause problems such as sudden extinguishment during the operation of the boiler. In severe cases, it may lead to the unit operating at a reduced load or even cause the boiler to shut down, directly affecting the safety of the boiler operation and the efficiency of the unit. Therefore, it is very important to establish a real-time monitoring system[24] that matches the ash deposition state of the boiler heating surfaces and optimize the soot blowing system [25]guided by the monitoring data. This plays an irreplaceable role in terms of safety and economy.

It can be seen that in the field of studying the fouling monitoring of the heating surfaces of alkali recovery boilers, it is very necessary to develop an intelligent control method that can avoid the shortcomings of the mechanism-based modeling method and the data algorithm-based modeling method. At the same time, this method can start the soot blowing according to the actual ash deposition degree of the boiler and the degree of decline in the heat transfer coefficient.

2. Materials

As a key component in the thermal energy recovery system, the heating surfaces of an alkali recovery boiler are not only the main areas for heat exchange but also the primary sites for dust accumulation. These heating surfaces are typically suspended inside the boiler by a suspender system to ensure their stable and efficient operation. When dust accumulates on the surface of the heating surfaces, it not only affects the heat exchange efficiency but also causes an increase in the suspension load borne by the suspenders. This increase in load may pose a potential threat to the structural integrity and operational safety of the boiler.

In view of the above situation, this study proposes an innovative approach, which is to indirectly determine the ash deposition situation on the heating surfaces of the alkali recovery boiler by analyzing the stress distribution and deformation characteristics of the boiler's suspenders. Additionally, through heat transfer experiments on the influence of ash deposition simulation on the heat transfer coefficient, the relationship between the deformation amount and the heat transfer coefficient is further explored. The core of this method lies in the fact that the change in the suspender load caused by ash deposition directly leads to changes in the stress distribution and deformation pattern of the suspenders. Therefore, by monitoring these changes, the ash deposition status of the heating surfaces can be effectively evaluated, enabling timely implementation of necessary ash removal measures to ensure the efficient and safe operation of the boiler. To achieve this goal, a mathematical model highly corresponding to the actual operating conditions was first established, and simulation software was used for simulation analysis. This model fully takes into account factors such as the material properties and geometric dimensions of the suspenders, ensuring the accuracy and reliability of the simulation results.

After preliminary analysis and verification, the model successfully reproduced the stress distribution and deformation characteristics of the suspenders under ash deposition conditions, demonstrating its feasibility as a basis for judging the ash deposition in the boiler. On this basis, a set of experimental equipment was further set up to conduct real-time monitoring and recording of the stress distribution and deformation characteristics of the suspenders, providing data for subsequent research.

2.1 Development of the experimental device for measuring the relationship between ash deposition weight and heat transfer coefficient

High-finned tubes used in high-efficiency heat exchangers are special-shaped tubes. They take plain tubes as blanks and form spiral fins on the outer surface of the tubes through rolling or pressing. They are mainly divided into single-metal high-finned tubes and bimetallic high-finned tubes. For single-metal high-finned tubes, the outer surface of the metal tube blank is processed into a fin shape, and the fins and the metal tube are an integral whole. Bimetallic high-finned tubes are composed of two kinds of metal tubes closely combined, and the outer surface of the outer metal tube blank is processed into a fin shape. High-finned tubes not only expand the heat exchange surface area but also promote the disturbance of the fluid, reduce the heat transfer resistance, effectively increase the heat transfer coefficient outside the tube, and thus greatly improve the efficiency of the heat exchanger. In the field of fin heat exchange in boilers, the heat transfer coefficient is a key indicator for measuring the heat transfer efficiency between the fins and the fluid. The theory of "Heat Transfer" clearly states that the heat transfer coefficient K represents the amount of heat transferred per unit time, through a unit area, and under a unit temperature difference. This parameter is crucial for evaluating the performance of boiler fin heat exchange, as it directly determines the efficiency of the heat exchange process and the related energy consumption.

Overall heat transfer coefficient as follows:

$$\frac{1}{U} = \frac{1}{h_i} + \frac{1}{h_o} + \frac{R_f}{A} + R_c, \qquad (2.1)$$

where
U − the overall heat transfer coefficient (W/m^2· K),
h_i − the convective heat transfer coefficient of the inner surface (W/m^2· K),
h_o − the convective heat transfer coefficient of the outer surface (W/m^2· K),

R_f − the thermal resistance of the solid wall material (K· m^2/W),

A − the heat exchange area of the heat exchanger (m^2),
R_c − the thermal resistance caused by the thermal conductivity and flow state of the fluid (R).

2.1.1. Heat transfer theorem of the ring pipe

The heat transfer behavior between the inner and outer walls of an annular pipe is described. When the temperature of the inner wall is constant, the heat flux density of the inner wall remains constant, while the heat flux density of the outer wall varies with changes in the outer wall temperature. This phenomenon is determined by radial heat conduction and convective heat transfer. The relationship as shown in Eqs. (2.2)–(2.4).

Internal heat flow density of the pipe wall:

$$q_i = h_i(T_i - T_f), \quad (2.2)$$

where
q_i – the heat flow density of the inner tube wall (W/m²),
h_i – the convection heat exchange coefficient of the inner tube wall (W/m²·K),
T_i – the internal pipe wall temperature (K),
T_f – the fluid temperature (K).

Heat flow density of the outer pipe wall:

$$q_o = h_o(T_f - T_o), \quad (2.3)$$

where
q_o – the heat flow density of the outer tube wall (W/m²),
h_o – the convection heat exchange coefficient of the outer tube wall (W/m²·K),
T_o – the external pipe wall temperature（K）

Heat transfer balance:

$$q_i \cdot A_i = q_o \cdot A_o, \quad (2.4)$$

where
$A_i = 2\pi r_i L$ – the surface area of the inner tube wall (m²),
$A_o = 2\pi r_o L$ – the surface area of the outer tube wall (m²).

2.1.2. Conduction thermal resistance

The conduction thermal resistance refers to the thermal resistance through the fins as follows:

$$R_{cond} = \frac{L}{k \cdot A}, \quad (2.5)$$

where
L – the thickness of the heat conduction path (m),
k – the thermal conductivity of the material (W/m·K),
A – the cross-sectional area of heat conduction (m²).

2.1.3. Radiative heat transfer

If the heat exchanger involves high-temperature surfaces, radiative heat transfer may also need to be considered, especially when there is a large temperature difference as:

$$Q_{rad} = \sigma \cdot A \cdot \epsilon \cdot \left({T_S}^4 - {T_\infty}^4\right), \quad (2.6)$$

where
σ – Stefan–Boltzmann constant ($5.67 \times 10^{-8} \mathrm{W/m^2K^4}$),
A – area of the radiating surface (m²),
ϵ – emissivity of the material,
T_S – surface temperature (K),
T_∞ – ambient temperature (K).

Combining these heat transfer processes, the heat transfer coefficient of the overall heat exchange can be expressed as:

$$K = Q/(A_0 \Delta T_m). \quad (2.7)$$

The formula for calculating the heat transfer coefficient of the measured tube can be obtained as follows:
– the heat transfer area:

$$A_0 = \pi dl, \quad (2.8)$$

– the heat transfer quantity:

$$Q = Gr, \quad (2.9)$$

– the amount of condensed water:

$$G = \frac{hg_s\gamma}{1000t \times 60}, \quad (2.10)$$

– the logarithmic mean temperature:

$$\Delta T_m = \frac{(T_1 - T_2)}{ln\frac{(T_1 - T_\infty)}{(T_2 - T_\infty)}}, \quad (2.11)$$

where:
d – outer diameter of the heat exchange tube (cm),
L – length of the measured heat exchange tube (cm),
r – latent heat of vaporization (J/kg),
h – water level height of the accumulator (cm),
g_s – condensate water amount per unit height (g/cm),
γ – specific weight of the condensed water (kg/m³),
T_1, T_2 – temperatures at both ends of the finned tube (K),
T_∞ – ambient temperature (K).

During the heat transfer process of spiral finned tubes, deposits such as dust and oil will gradually accumulate on the fin surface. These deposits will have a negative impact on the heat exchange effect. The accumulation of the dust layer increases the surface thermal resistance, leading to a decrease in the heat transfer coefficient. As the dust accumulation intensifies, the surface heat transfer efficiency decreases, thus affecting the overall thermal efficiency of the heat exchanger.

In an actual heat exchanger system, the heat transfer coefficient K generally decreases as the degree of surface dust accumulation (i.e., the amount of dust deposition)S_{ash} increases. The influence of the degree of surface dust deposition can be approximately represented by an empirical formula:

$$K_{eff} = K_0\left(1 - \alpha S_{ash} + \beta {S_{ash}}^2 - \gamma {S_{ash}}^3\right), \quad (2.12)$$

where:

K_{eff} – effective heat transfer coefficient after ash deposition (W/m²·K),

K_0 – initial heat transfer coefficient when there is no dust deposition (W/m²·K),

S_{ash} – dust accumulation mass (g),

α, β, γ – a constant related to the dust accumulation situation. Usually, it is fitted through experimental data or empirical formulas, and the specific value is determined according to the actual system.

The research team reproduced the complex heat exchange scenarios during the actual combustion process of the boiler in a highly simulated environment through comprehensive heat transfer performance experiments. In the experiment, dry saturated steam was used as the heat source. As these steam passed through the specially designed copper finned tube radiators, the heat transfer process between the high-temperature steam inside the boiler and the external environment was simulated. As the steam flowed inside the finned tubes, the heat it carried was gradually released to the outside, causing the steam temperature to gradually decrease. Eventually, the steam condensed into water on the surface of the finned tubes. This process well reflected the essence and effect of heat transfer.

The core of this experiment is to explore how the surface condition of the finned tubes and the air flow conditions subtly affect the heat transfer efficiency. The study has found that factors such as the cleanliness of the finned tube surface, the distribution and thickness of dust accumulation, as well as the velocity, temperature and humidity of the surrounding air, all have a significant impact on the heat transfer process. These factors not only change the surface area of heat transfer and the characteristics of the boundary layer, but also affect the condensation effect and the amount of condensed water per unit time, thus becoming key parameters for evaluating the heat transfer performance.

By statistically analyzing the changes in the amount of condensed water under different conditions, and based on these data, the total heat transfer coefficient K value of the finned tubes under different dust accumulation states was calculated using the principles of heat transfer and relevant formulas. The calculation results visually demonstrate the negative impact of dust accumulation on the heat transfer performance, providing strong data support for a deep understanding of the heat transfer mechanism and the optimization of boiler design. The experimental setup is shown in Fig. 1.

Fig. 1. Heat transfer experimental setup.

2.2 **Development of the dust accumulation weight detection device**

In practical applications, the heating surface of the boiler is suspended on the crossbeam. When the boiler is operating, the heat exchange tubes of the heating surface are filled with water. After the pulverized coal in the boiler enters the furnace, it is entrained and burned by the high-temperature flame to produce coal ash. The molten or semi-molten fly ash, entraining the dust generated by combustion, adheres to the heating surface. Slagging and dust accumulation on the heating surface will cause an increase in the weight of the heating surface. The suspension rod will undergo a slight deformation along the axial direction as the weight changes. According to Hooke's law in the mechanics of materials: in the elastic deformation stage of metal materials, stress and strain are linearly related. The relationship between stress and strain can be expressed as:

$$\sigma = E \cdot \varepsilon, \tag{2.13}$$

where

σ – stress (Pa),

E – elastic modulus of steel is a constant value ($E = 2.06 \times 10^5$Pa)

ε – strain(με)，$1\mu\varepsilon = 10^{-6}$,

and

$$\sigma = \frac{N}{A}, \tag{2.14}$$

N – applied load, with the unit of Newton (N)

A – cross-sectional area of the suspension rod (m²).

During the mechanical experiment, in order to accurately measure and quantify the deformation behavior of the suspension rod under tensile force, an integrated testing system was adopted. This system combines a high-precision mechanical experimental platform, strain gauge sensors, and an advanced deformeter. By applying tensile force on the high-precision mechanical experimental platform, the suspension rod undergoes corresponding deformation. At the same time, the strain gauge sensors pasted on the surface of the suspension rod change and transmit signals to the deformeter. The weak signals are amplified simultaneously, enabling the reading of corresponding data.

2.2.1 Selection of the acquisition device

In view of the problem of inaccurate detection of the heating surface, this paper intends to develop a device that can detect the degree of dust accumulation on the heating surface in real time to assist in precise soot blowing. Therefore, the actual working conditions of the factory were investigated, and an experimental device was designed by simulating the site. Considering that the increase in the weight of dust accumulation on the heating surface will cause an increase in the axial load of the suspension rod, it was decided to reflect the degree of dust accumulation on the heating surface by detecting the change in the weight load borne by the suspension rod. Through preliminary analysis, two measurement methods are available: using a load sensor and pasting strain gauges on the suspension rod, And a comparison was made to select between the two methods, as shown in Fig. 2.

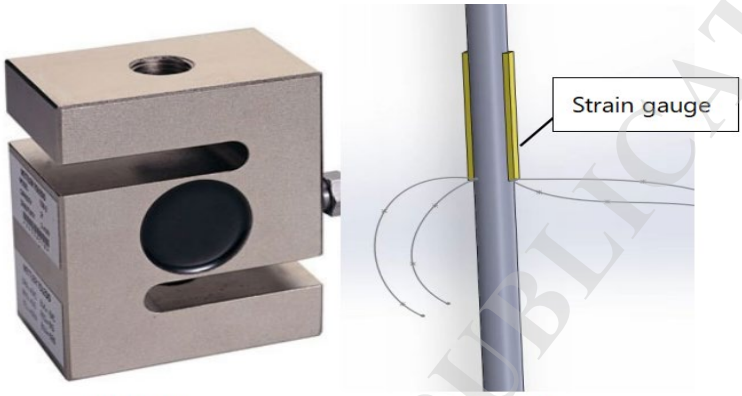

Figure(a) S-type load sensor

Figure(b) Paste strain gauges

Fig. 2. Schematic diagram of scheme comparison.

As shown in Fig. 2a, an S-shaped sensor was adopted. The S-shaped sensor offers high precision, stability, and strong anti-interference capabilities. Its compact size makes it easy to install in various space-constrained situations and reduces the additional burden on surrounding equipment. However, the sensor must be precisely suspended on the main suspension rod. This specific installation requirement not only increases the initial installation difficulty but also causes inconvenience during subsequent maintenance or when the sensor needs to be replaced. Moreover, the S-shaped sensor has certain limitations in terms of its frequency response range. For application scenarios requiring rapid response or high-frequency measurements, its performance may not fully meet the requirements. Additionally, the installation process is inconvenient, as it requires complete disassembly of the system for installation.

As shown in Fig. 2b, The method of directly attaching strain gauges was adopted, as shown in Fig. 2b. As a highly sensitive sensor element, strain gauges can tightly adhere to the surface of measured objects with complex curvatures. They can make good contact and attach to one side of the suspension rod, capturing minor strain changes on the surface of the measured object and converting them into electrical signals. This process offers high precision and rapid response, accurately reflecting the strain conditions of the measured object and providing real-time monitoring capabilities. Additionally, installation and replacement are convenient, as there is no need to disassemble the entire system; the strain gauges can be directly replaced and attached at the suspension rod. However, temperature changes are one of the main factors affecting their measurement accuracy. Since the resistance value of strain gauges varies with

temperature, when the measured object is in an environment with significant temperature fluctuations, the measurement results of the strain gauges may be subject to some degree of interference.

Through the analysis and comparison of the two schemes, the scheme of directly pasting strain gauges was finally adopted. In order to eliminate the influence of temperature changes, strain gauges with built-in temperature compensation were selected to ensure the accurate measurement of the strain caused by the applied force.

2.2.2 Suspension rod loading device

To accurately simulate and evaluate the stress distribution and deformation characteristics of the suspension rods of the heating surface of the alkali recovery boiler, 20 steel (C 0.17-0.23, Si $\leq$ 0.17, Mn:0.35 ~0.65, P $\leq$ 0.035, S $\leq$ 0.035), which is widely used in the industry, was selected as the material for the suspension rods. The intention is to precisely replicate the stress conditions in the actual working environment. The diameter of the suspension rod is 55 *mm*, and its length is 380 *mm*. To ensure the accuracy of the experimental results, holes with a diameter of 15 *mm* perpendicular to each other were designed at both ends of the suspension rod. The purpose is to reduce the impact of stress concentration on the measurement results when tensile force is applied. To ensure the smooth progress of the experiment, 45 steel (C 0.42-0.50，Si 0.17-0.37， Mn 0.50-0.80，P $\leq$ 0.035，S $\leq$ 0.035) with high load-bearing capacity was chosen to manufacture the base and the upper seat. At the left and right ends of these components, holes with a diameter of 15 *mm* corresponding to those of the suspension rod were also designed. The suspension rod and the base are fixedly connected by dowel pins. This not only ensures stability but also guarantees that the suspension rod has appropriate degrees of freedom in the x and y directions. It effectively prevents the suspension rod from breaking or deforming due to stress concentration and significantly reduces experimental errors.Finally, the base is firmly fixed to the experimental bench with bolts and nuts, thus completing the construction of the entire experimental device. The entire construction process strictly adheres to international safety standards and operating procedures, ensuring the safety and reliability of the experimental device. This provides a guarantee for the subsequent in-depth exploration and optimization of the performance of the suspension rods of the alkali recovery boiler. The structure is shown in Fig. 3.

Fig. 3 Suspension rod loading device.

2.3 Experimental design and setup of the device

In the research on the stress distribution and deformation characteristics of the suspension rods of the alkali recovery boiler, experimental design is of crucial importance. To ensure measurement accuracy and data reliability, a resistive strain gauge with a large resistance value of 350 ohms was first selected. Due to its high sensitivity and long-term stability, this type of strain gauge demonstrates excellent performance in capturing the stress changes of the suspension rod under various complex working conditions. It is especially suitable for high-temperature working environments, providing a solid hardware foundation for the experiment. In the experimental design, the middle ring wall position of the suspension rod was chosen to paste the strain gauges to accurately measure the strain of the suspension rod.

To reduce experimental errors and balance the Wheatstone bridge, a reference control group was set up. The control group consists of the same suspension rods as those in the experimental group. Strain gauges of the same specifications are pasted on them under the unloaded state and then connected to the *XL2118A* static resistive strain gauge. By measuring and recording the strain data of the suspension rod in a stationary state, an accurate baseline is provided for the subsequent data under the loaded state, effectively eliminating the errors that may be introduced by environmental factors or the equipment itself.

During the setup of the experimental device, first, the strain gauges were precisely pasted on the middle sidewall of the suspension rod. Then, bolts and pins were used to firmly connect the suspension rod to the mechanical loading test bench, forming a complete and reliable testing system. According to the principle of electronic measurement, the leads of the strain gauges were connected to the corresponding ports of the static resistive strain gauge according to the standard single-bridge circuit connection method. At the same time, to ensure the rigor of the experiment and the reliability of the data, the suspension rod of the control group and its strain gauges were also connected to the strain gauge in the same way to achieve synchronous monitoring and comparative analysis. The structure is shown in Fig. 4.

Fig. 4 Schematic diagram of the tensile force application platform:
1. strain indicator, 2. mechanical loading platform, 3. temperature compensator,
4. strain gauge, 5. suspension rod.

2.3 Final application of the simplified model

The ultimate goal of this paper is to develop a device based on strain gauge monitoring technology. By attaching strain gauges to the suspension rods, the device can capture the deformation of the rods caused by the accumulation of ash on the heating surface in real time. By monitoring the degree of deformation, the device determines the ash accumulation status and triggers corresponding cleaning mechanisms, ensuring that the heat transfer efficiency of the heating surface remains within the high-efficiency range. As shown in Fig. 5.

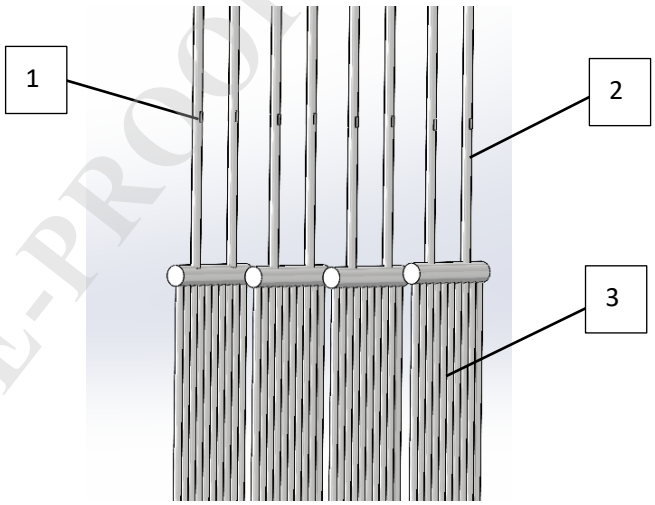

Fig. 5. Practical application scenarios:
1. Strain gauge, 2. suspension rod, 3. heating surface.

3. Methods

3.1 Simulation of the ash deposition process

Excessive ash deposition will reduce the heat transfer efficiency of the boiler. Since the thermal conductivity of the ash layer is much lower than that of the metal pipe wall, ash deposition seriously affects the heat transfer inside and outside the heating surface, resulting in a decline in the boiler's heat transfer efficiency. It will also increase the flue gas temperature. As the heat transfer efficiency drops, the flue gas temperature will rise, which may further trigger more serious high-temperature ash deposition and large-scale coking. Moreover, it will increase the operating cost. When the ash deposition is severe, the boiler needs to be shut down for cleaning and maintenance, which will cause production disruptions and thus increase the operating cost.

In the ash deposition simulation experiment, an electric heating steam generator was used to replace the combustion and heat transfer process of the recovery boiler. The system was scaled down proportionally for the experiment. The main components of the ash in the actual ash deposition process include unburned carbon, inorganic minerals, and other impurities such as sulfur oxides and carbonates. It is quite difficult to simulate the actual ash deposition situation during the actual operation. Therefore, choosing gypsum liquid as a simulation material is a relatively reasonable alternative, which can simulate some characteristics of actual ash deposition to a certain extent. (The slurry formed after preparing the gypsum mixture will gradually harden during the drying process, forming a solid layer similar to the ash deposit, which can simulate the physical form and adhesion of the actual ash deposition. Gypsum powder has good adhesion, and this property can simulate the characteristics of actual ash deposition that accumulates on the surface of objects for a long time and is difficult to clean. Meanwhile, gypsum materials have a certain degree of hygroscopicity, which can simulate the phenomenon of actual ash deposition absorbing moisture, increasing in weight and volume in a humid environment. The prepared slurry has a high degree of controllability in terms of proportioning, coating thickness, and drying conditions, etc., and can simulate ash layers with different thicknesses, densities, and hardnesses as required).

First, design the ratio of gypsum to water. Conduct small-scale preliminary experiments first. Prepare gypsum slurries with different ratios, smear them, and observe their surface adhesion and whether a stable ash deposition layer can be formed. Finally, the optimal ratio is determined to be gypsum: water = 1:0.5. Weigh gypsum powder and water strictly according to the ratio of 1:0.5 for preparation. After stirring evenly, use a paintbrush to smear the mixture evenly on the heat dissipation pipe. Let it stand and air dry naturally until it gradually hardens. When conducting the experiment, the dust distribution state is as shown in Figure 6.

Fig. 6. Schematic diagram of ash deposition distribution.

3.2 Experimental method for measuring the relationship between ash deposition weight and heat transfer coefficient

(1) Before operating the electric heating steam generator, first ensure that there is enough water in the boiler of the steam generator. Open the water supply valve and exhaust valve on the electric heating steam generator to add water to the boiler of the steam generator. When the water level reaches two-thirds of the height of the water level gauge, close the valves.

(2) Turn on the electric heater switch on the steam generator. The automatic 6kW indicator light turns on, and the steam generator starts heating. When the electric contact pressure gauge reaches the required pressure value of 0.3 MPa, the electric contact pressure gauge cuts off the power. At this time, the electric contact pressure gauge controls the relay to make the heater heat within a certain range to supply the steam amount required for the experiment.

(3) Open all the valves on the steam distribution pipe and the drain valve below the glass water accumulator. Open the steam supply valve and slowly send steam into the test tube to preheat the entire experimental system and exhaust the air in the system.

(4) After the drain valve at the bottom of the water accumulator discharges steam for a period of time, close all the drain valves. The preheating is completed. Adjust the drain valve at the bottom of the steam distribution pipe to make it emit steam slightly to drain the condensed water in the rubber tube. Adjust the steam supply pressure, and then the experiment can start. To prevent the glass water accumulator from being damaged, the experimental pressure is 0.2 MPa, and the maximum should not exceed 0.3 MPa.

(5) Conduct a forced convection experiment. Drain the water accumulated in the accumulator and pipelines. Start the fan to conduct forced convection ventilation on the test pipeline. Pay attention to the water level change in the water accumulator. Start timing when the water level rises to the “0” position. The experiment officially begins. When the condensed water level reaches a certain height, record the steam supply time and the change data of the condensed water volume to calculate the heat transfer coefficient.

(6) When the experiment is completed, turn off the power supply, open all the drain valves and steam release valves. After the water is completely drained, close all the valves, and cut off the power supply and water source.

During the experiment, it is necessary to record the temperatures inside and outside the pipe corresponding to different ash deposition states, the initial liquid level, and the final liquid level.

Finally, obtain the temperature difference inside and outside the finned pipe and the amount of condensed water for the calculation of the heat transfer coefficient.

3.3 Research and analysis of the relationship between weight load and strain

The tensile force is applied to it through a mechanical testing machine, and the amount of deformation generated under different working conditions of tensile force application is measured. The steps are as follows:

(1) After the entire device is set up, first set the parameters of the strain gauge. Adjust the sensitivity, range, and filter of the strain gauge and perform zero adjustment to eliminate the initial errors of the instrument itself.

(2) According to the preset loading rate and tensile force range, gradually increase the tensile force from zero to 5000 *N* at a stable and controllable speed. Ensure the uniformity of the tensile force increase rate to avoid sudden impact or overloading on the sample.

(3) While applying the tensile force, use the strain gauge to monitor the deformation of the sample in real time, and accurately record the corresponding deformation amounts under different tensile force values through the data acquisition system. High-resolution sensors and high-speed data acquisition technology are adopted to ensure the accuracy and real-time nature of the data.

(4) After completing the tests at all the predetermined tensile force points, gradually reduce the tensile force to zero according to the operating procedures, and stop the operation of the mechanical testing machine.

4 Results

4.1 Heat Transfer Efficiency

First, take 0g, 200g, and 400g as examples to analyze the results of the ash deposition heat transfer determination device. The results are shown in Figure 7 and Tables 1–3.

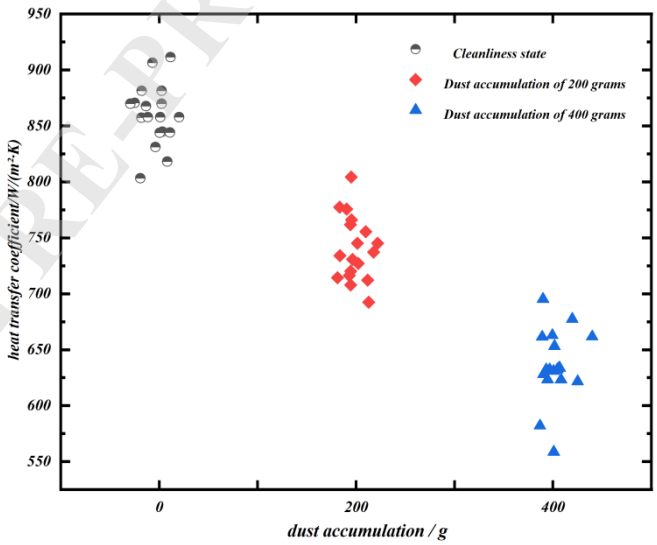

Fig. 7. Distribution map of heat transfer coefficient of ash deposition.

Table 1. Heat transfer coefficient table corresponding to 400 g of ash deposition

Inlet temperature [°C]	Outlet temperature [°C]	Initial liquid level [ml]	Final liquid level [ml]	Wind speed [m/s]	Heat transfer coefficient [W/(m²·K)]
126	96	0	251	5.2	695.28
129.5	94.8	0	285	5.4	662.92
136	105.2	0	210	5.1	582.1
131	108	0	155	5.2	558.63
128	103	0	190	5.1	633.72
135	108.4	0	205	4.9	632.26
128	99.8	0	235	5.1	621.72
135.1	109	0	210	5.2	677.52
133.9	110	0	180	4.8	653.16
129.3	104.3	0	195	5.2	633.72
131.9	102	0	210	5.1	628.13
136.5	110.5	0	205	5.3	661.46
133.7	107.7	0	205	5.2	630.95
136.3	112.3	0	180	5.3	623.26
128.5	105.5	0	175	5.1	632.29
131.3	104.3	0	215	5.2	661.73
136.5	112.4	0	180	5.0	623.26
127.4	104.4	0	175	5.1	632.29

Table 2. Heat transfer coefficient table corresponding to 200 g of ash deposition.

Inlet temperature [℃]	Outlet temperature [℃]	Initial liquid level [ml]	Final liquid level [ml]	Wind speed [m/s]	Heat transfer coefficient [W/(m²·K)]
137	104	0	300	5.2	755.47
128	99	0	250	5	716.38
131.1	101.1	0	275	5.1	761.76
137	109	0	245	5.2	727.13
130.4	102.5	0	240	5.3	712.29
129.3	100.5	0	260	5.1	745.04
130.2	99.2	0	300	5.2	804.22
130.3	99.4	0	290	5.1	777.39
131.1	104.1	0	230	5.2	707.89
128.7	98.7	0	280	5.1	775.61
135.2	104.2	0	275	5.3	737.18
133	103	0	260	5.2	720.21
133.1	101.2	0	295	5.2	766.08
136.6	107.5	0	260	5.1	745.04
129.2	101	0	235	5.3	692.51
134.2	104	0	265	5.3	734.05
136.8	107.8	0	255	5.2	730.71
131.9	103.4	0	245	5.4	714.37

Table 3. Heat transfer coefficient table corresponding to the clean state.

Inlet temperature [℃]	Outlet temperature [℃]	Initial liquid level [ml]	Final liquid level [ml]	Wind speed [m/s]	Heat transfer coefficient [W/(m²·K)]
127.1	94	0	350	5.1	881.37
131.2	99.2	0	349	5.2	906.31
135.5	101.5	0	355	5.3	867.67
135	104	0	320	5.2	857.81
127.5	97	0	330	5.2	870.58
132.2	102.2	0	305	5.1	844.86
128	97.5	0	305	5.1	831.01
130.5	100.5	0	290	5.2	803.31
129.8	98.8	0	320	5.2	857.81
135.6	104.1	0	320	5.3	844.21
132.7	101.2	0	3 25	5.2	857.39
127.3	95	0	335	5.1	869.96
137.2	105.2	0	315	5.2	818.02
130.8	99.8	0	340	5.3	911.43
132.5	101.5	0	320	5.1	857.81
129.8	97.8	0	325	5.2	843.98
135.7	103.7	0	335	5.2	869.96
127.1	94	0	350	5.1	881.37

(1) Under the condition that the velocity, temperature, and humidity of the surrounding air remain constant, and only the cleanliness of the finned tube surface, the distribution, and thickness of the ash deposition are changed, through the analysis of the data obtained from the heat conduction experiments under three different ash deposition states, it is found that as the degree of ash deposition gradually increases, the steam temperature decreases more slowly. This leads to a reduction in the amount of accumulated water, thereby reducing the heat transfer coefficient.

(2) The data analysis shows that when the ash deposition amount reaches 400g, the heat transfer coefficient is restricted to a relatively low range of 600 to 700 W/(m²·K). When the ash deposition amount is halved to 200g, the heat transfer coefficient increases to the range of 700 to 800 W/(m²·K). Most significantly, when the surface of the finned tube remains clean without ash deposition, the heat transfer coefficient reaches its optimal value, ranging from 800 to 900 W/(m²·K). This series of data clearly reveals the influence of the degree of ash deposition on the heat transfer efficiency, indicating an inverse relationship between the ash deposition weight and the heat transfer coefficient. That is, as the ash deposition weight increases, the heat transfer coefficient gradually decreases.

In order to obtain the relationship between the heat transfer coefficient and the amount of ash deposition more accurately, a heat transfer experiment was conducted for every 20 g increase in the amount of ash deposition within the range of 0 to 400g, with 20 g as the unit. The experimental results are shown in Table 4.

Table 4. corresponding table of heat transfer coefficients at equal gradients for ash deposition amounts ranging from 0 to 400 g.

Dust mass [g]	Average heat transfer coefficient [W/(m²·K)]
0	863.44
20	861.86
40	862.21
60	860.39
80	857.62
100	849.49
120	838.56
140	832.22
160	823.61
180	814.31
200	795.75
220	772.17
240	760.17
260	744.36
280	725.21
300	704.66
320	691.73
340	673.6
360	660.73
380	642.31
400	627.31

(1) By observing Table 4, the relationship equation between the experimental heat transfer coefficient and the amount of ash deposition can be fitted as shown in Fig. 8. The obtained equation is as

$$y = 859.767 + 0.25X - 0.0038X^2 + 4.295 \times 10^{-6}X^3, \quad (4.1)$$

where y is the heat transfer coefficient [W/m^2·K] and X is the dust accumulation mass [g].

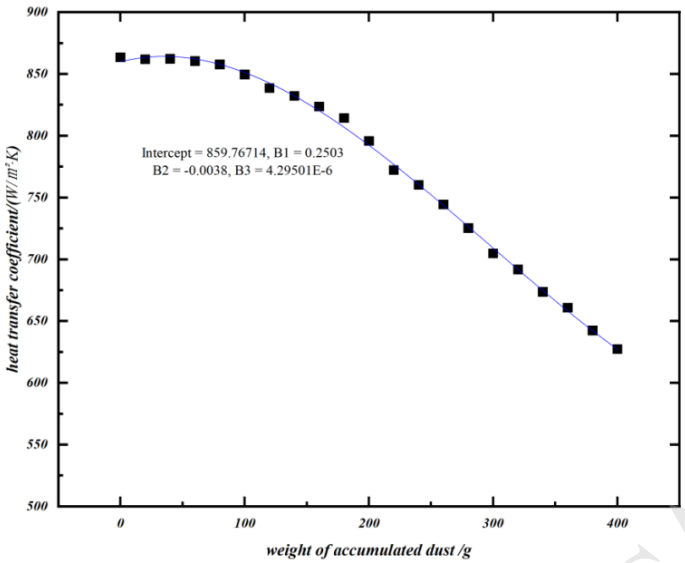

Fig. 8. Curve graph of heat transfer coefficient distribution.

(2) By taking the second derivative of it, the inflection point is found to be at X = 294.77 g. That is, when the ash deposition weight reaches 294.77 g, the downward trend of the heat transfer coefficient will change, affecting the heat exchange.

In the initial stage of ash deposition, when the amount of ash deposition is in the range of 0 to 294.77g, the decline rate of the heat transfer coefficient gradually slows down. When the ash deposition weight reaches 294.77 g, the downward curve will tend to be stable. At the same time, taking this point as the boundary, the concavity and convexity of the curve will also change. In the later stage, when the amount of ash deposition is in the range of 294.77 to 400 g, the decline rate of the curve will increase, and the heat transfer coefficient will drop significantly, having a great impact on the heat transfer effect. Therefore, starting the soot-blowing device before the inflection point to remove ash can ensure the overall efficient operation.

(3) Meanwhile, this equation can also indicate the adverse effect of the ash deposition phenomenon on the thermal performance of the system. Given the negative impact of ash deposition on the heat transfer efficiency, it is very important to develop highly efficient and accurate ash deposition detection devices and implement regular or timely ash cleaning and maintenance strategies to maintain the cleanliness of the heat dissipation surface and ensure the efficient operation of the system.

4.2 Tensile Test

The experiment was conducted using a mechanical loading test bench, and the corresponding deformations under different tensile forces were measured, as shown in Fig. 9.

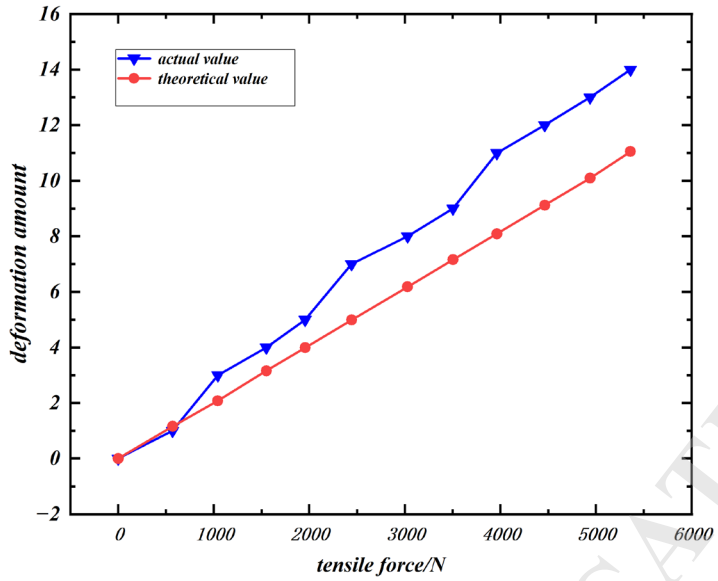

Fig. 9. Tensile force – deformation diagram.

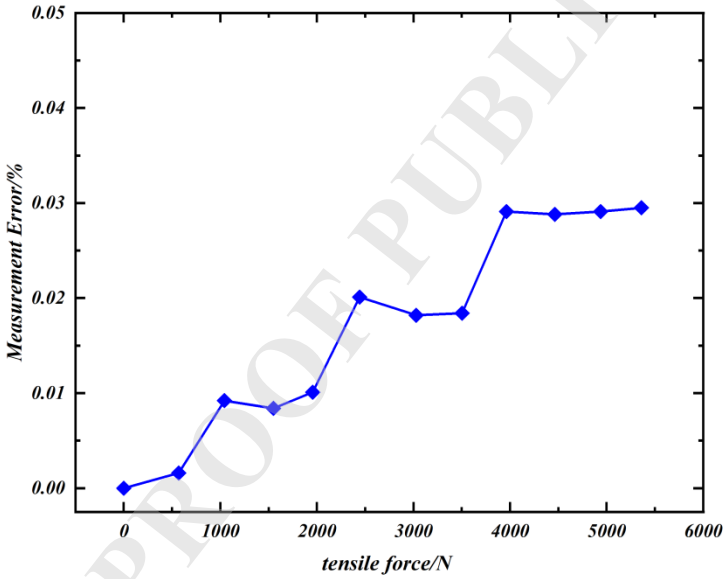

Fig. 10. Strain error analysis under different load conditions.

By observing the generated deformation and calculating the change of deformation with the applied load, the following points can be obtained.

(1) In the initial state, when the applied load is 0, both the generated deformation and the calculated deformation are close to zero. This indicates that the object maintains its original shape without deformation when there is no external force. As can be seen from the figure, whenever the load increases from 500N to 600N, a corresponding deformation is added, and there is a good linear relationship between the two.

(2) As the applied load increases, both types of deformations start to increase. The red curve (calculated deformation) may be slightly higher or lower than the gray curve (generated deformation) at some points, but overall, they maintain a very close trend. This closeness indicates that the theoretical model has a high degree of accuracy in predicting the object's deformation. Although the two curves are very close, there are still slight differences. For

example, when the applied pressure is 1549 N, the measured deformation is 4με, and the theoretically calculated deformation is 3.16με. This is because the data measured by the experimental equipment has a certain range, and the values are represented as integers rather than decimals. Therefore, there is a one-to-one correspondence between the deformation data values measured by the experimental equipment under different tensile forces and the deformations obtained through theoretical calculations as shown in Fig. 10, the strain measurement maintains a maximum 0.05 % deviation from theoretical values throughout progressive loading, demonstrating high precision with insignificant error influence.

(3) In conclusion, although there may be slight numerical differences between the generated deformation and the calculated deformation, they show a high degree of linear similarity in the overall trend of changing with the applied load. This closeness indicates that the method of pasting strain gauges has a high degree of accuracy in predicting the object's deformation, can capture the deformation well, and provides strong support for practical applications.

4.3 Corresponding Relationship

In actual operating conditions, when the ash deposition weight reaches 500 kg, it usually reaches the critical value for soot blowing and cleaning. When the heat exchange tube used in the heat transfer experiment is scaled up to be the same as the heat exchange surface carried by the suspender in actual operating conditions, that is, scaled up by a factor of 1250, it can correspond to the actual operating conditions, and The corresponding relationship as shown in Table 5 is obtained.

Table 5. Corresponding table of strain and heat transfer coefficient.

Tensile force [N]	Dust mass [g]	Strain [με]	Heat transfer coefficient [W/m^2·K]
0	0	0	859.77
568	45	1	863.73
1042	83	3	856.83
1549	123	4	841.05
1955	156	5	842.57
2442	195	7	795.86
3027	242	8	758.73
3503	280	9	725.15
3962	316	11	694.37
4463	357	12	660.03
4937	394	13	631.66
5360	428	14	607.73

(1) By reducing the experimentally measured tensile force in equal proportion, the corresponding ash deposition weight on the heat transfer finned tube can be obtained. Through the equation fitted from the data in Table 4, the heat transfer coefficient corresponding to the

ash deposition state can be calculated. The heat transfer coefficient can be correlated with the deformation corresponding to the applied tensile force one by one. It can be observed that as the ash deposition weight gradually increases, the corresponding deformation also gradually increases. At the same time, the heat transfer coefficient gradually decreases. The two show a good inverse relationship, that is, the heat transfer coefficient decreases as the generated strain increases.

(2) By taking the derivative of the equation corresponding to the ash deposition state and the heat transfer coefficient, the inflection point is found to be at an ash deposition weight of 294.77 g. As analyzed in Section 4.2, a continued increase in the ash deposition amount after the inflection point will have a significant impact on the heat transfer coefficient. Therefore, the soot-blowing device must be started before the inflection point. Corresponding 294.77 g to Table 5, it can be seen that when the ash deposition amount reaches 280 g, it is closest to the ash deposition amount at the inflection point and is before the inflection point. Therefore, it is most reasonable to perform the soot-blowing operation at this moment.

(3) When the ash deposition amount reaches 280 g, according to the corresponding relationship in the table, in actual operating conditions, when the ash deposition weight reaches 3503N, the corresponding deformation of the suspender is 9 με, and the heat transfer coefficient is 725.15 W/(m²·K). Starting the soot-blowing device at this time can avoid steam waste caused by excessive soot blowing and the decline in heat transfer efficiency due to untimely soot blowing. This further verifies the feasibility of pasting strain gauges on the main suspender to monitor the ash deposition weight.

5 Conclusions

This study focuses on the efficient and energy-saving operation of recovery boilers in the paper industry. Specifically, it addresses the pain point that the traditional time-based soot-blowing system cannot flexibly adjust the soot-blowing frequency according to the real-time ash deposition status, resulting in energy waste. By innovatively proposing the integration of strain gauge detection technology on the main suspender, the dynamic monitoring and quantitative evaluation of the ash deposition weight on the heat absorption surface of the boiler have been achieved.

Firstly, through comprehensive heat transfer performance experiments, the complex heat exchange scenarios during the actual combustion process of the boiler were reproduced. In the heat transfer performance experiments, particular attention was paid to the subtle influences of the surface state of the finned tubes, the cleanliness of the finned tube surface, the distribution of ash deposition, and the air flow conditions on the heat transfer efficiency. The experimental results show that the cleanliness of the finned tube surface, the distribution and thickness of ash deposition, as well as the flow velocity of the surrounding air, have a significant impact on the heat transfer process. They not only change the surface area of heat transfer and the characteristics of the boundary layer but also greatly affect the heat transfer efficiency.

Then, through numerical calculations and finite element simulation analyses, an in-depth comparison was made between the experimental data and theoretical predictions. The results show that the error rate between them was controlled within a very low percentage range, which fully demonstrates the accuracy and reliability of this method. Finally, the experimental results indicate that when the ash deposition load reaches 500 kg, the strain gauges on the suspender

can accurately capture a strain increment of 14 με, and there is a highly linear relationship between this strain change and the ash deposition weight.

Finally, by studying the corresponding relationship between the deformation amount and the heat transfer coefficient, the point at which the heat transfer coefficient begins to play a significant role corresponding to the ash deposition state and its corresponding ash deposition amount were obtained. It was concluded that the optimal point to start the soot-blowing process is when the ash deposition amount reaches 3503 N and the strain is 9με. This discovery not only verifies the feasibility and accuracy of using strain gauges as sensors for monitoring ash deposition amount but also lays a solid foundation for subsequent data processing and algorithm development.The specific implementation process is shown in Figure 5.1.

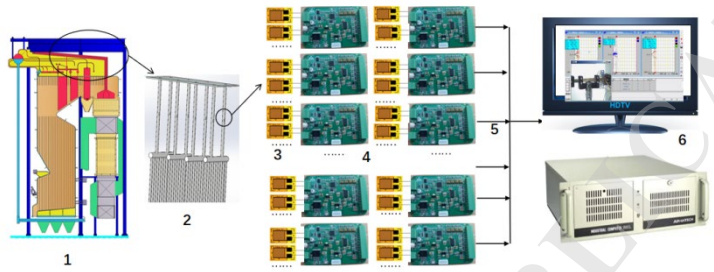

Fig. 11. Strain working principle diagram: 1. alkali recovery boiler, 2. ash accumulation detection device, 3. strain gauge, 4. signal acquisition and amplification circuit, 5. transmission bus, 6. signal processing software system.

As shown in Fig. 11, the strain gauge-based ash monitoring system for the heat absorption zone of a recovery boiler proposed in this study has been applied in practical engineering applications. By installing high-precision strain gauges at key load-bearing positions near the heat-absorbing surface of the boiler, a comprehensive online ash accumulation monitoring system is established. This system utilizes a multi-channel strain measurement module, where signals from each measurement point are transmitted via shielded twisted-pair cables to an integrated stress amplification and data acquisition microcontroller. After 24-bit high-precision ADC conversion and digital filtering, the data is uploaded to the central control unit via an industrial Ethernet communication protocol. The control unit employs software algorithms to perform trend analysis, data logging, and storage. The real-time strain data is dynamically converted into ash layer thickness distribution on the heat-absorbing surface using a load-strain mathematical model. When a preset threshold is detected, the system automatically triggers an intelligent soot-blowing control strategy to achieve efficient ash removal.

In conclusion, the method proposed in this study of pasting strain gauges on the main suspender to monitor the ash deposition weight can effectively address the problems of untimely or overly frequent soot blowing in traditional soot-blowing systems. It can significantly reduce the number of ineffective soot-blowing operations, decrease the steam consumption during the soot-blowing process, thereby reducing the overall energy consumption of equipment operation and enhancing the operational efficiency and economic viability of recovery boilers. The application of this innovative technology provides a new approach for

energy conservation and emission reduction in the pulp and paper industry. It also offers important theoretical support and technical references for the research, development, and promotion of intelligent soot-blowing systems for boilers. With the continuous maturation and optimization of the technology, this method will demonstrate its application potential and value in more fields.

This pilot application plan selects the heat exchange surfaces of recovery boilers as the target application scenario to achieve quantitative monitoring of fouling levels on boiler heating surfaces. The three-phase implementation ensures technical reliability: phase 1 involves a 3-month laboratory pre-validation, completing 20 sets of scaled-model soot-blowing tests and establishing a fouling detection database; phase 2 consists of 6 to 12 months of field testing to verify baseline performance of critical components and measurement stability across varying temperatures; phase 3 focuses on operational refinement. All validation metrics strictly comply with international standards, enabling precise management of soot-blowing system operation and performance optimization.

Project funding:
Shaanxi Province Science and Technology plan project（2024QCY-KXJ-006）.
PhD Research Initiation Project of Shaanxi University of Science and Technology, 2018BJ-28.

References

[1] Zhuang, H. Y. Energy - Saving and Efficiency - Enhancing Technologies for the Soot - Blowing System of the Recovery Boiler [J]. China Pulp & Paper Industry, 2024, 45(01): 43 - 45.
[2] Wahid S N ,Mustafa S M ,Arifin M N , et al.Hybrid nanofluid radiative flow across a permeable convective moving surface with heat generation: Numerical and statistical approach[J].Neural Computing and Applications,2024,(prepublish):1-13.
[3] Xu, L. G., Huang, Y. J., Wang, J., Yue, J. F., Zou, L., & Yang, Z. Optimization of Soot Blowing Based on the Furnace Slagging Monitoring Model [J]. Journal of Southeast University (Natural Science Edition), 2018(01).
[4] Benbeghila A ,Ouzani R ,Benderradji A , et al.Investigation of asymmetric heating in Poiseuille-Rayleigh-Bénard water flow: A numerical study[J].International Communications in Heat and Mass Transfer,2025,160108404-108404.
[5] Richard W, Kephart J J, et al. Boiler cleaning sootblower scheduling optimization[C] International Joint Power Generation Conference and Exposition and the International Conference on Power Engineering, USA.1999: 25-28.
[6] Pena B, Teruel E, Diez L I. Soft-computing models for soot-blowing optimization in goal-fired utility boilers[J]. Applied Soft Computing, 2011,11(2): 1657-1668.
[7] Koryakova MD,Nikitin VM,Speshneva NV,et al.Fouling and Corrosion of High-Alloyed Steel in Seaport Water[J].Protection of Metals,2001,37(3):249-253.
[8] Workshopon Intelligent Sootblowing Application[P].EPRI,1999
[9] Mayoral M C,Izquierdo M T,Andrs J M,et al.Mechanism of interaction of pyrite with hematite as simulation of slagging and fireside tube wastage in coal combustion [J]. 2002,390:103-111.

[10] Valero A,C Cortés.Ash fouling in coal-fired utility boilers Monitoring and optimization of on-load cleaning[J].Progress in Energy&Combustion Science,1996,22(2):189-200.
[11] Zhang S,Shen G,An L,et al.Ash fouling monitoring based on acoustic pyrometry in boiler furnaces[J].Applied Thermal Engineering,2015,84:74-81.
[12] Yang, X. H. Economic Research on the Optimization of Soot Blowing for 300MW Unit Boilers [J]. Boiler Technology, 2013(1): 15 - 18.
[13] Raza Q ,Wang X .Numerical simulation of Boger nanofluids with heat source, magnetic field, and Cattaneo–Christov heat flux model between two parallel permeable porous plates via finite difference method[J].Case Studies in Thermal Engineering,2024,64105518-105518.
[14] M. A ,I. R ,S. S .Enhancing heat transfer efficiency and energy improvement through novel biosynthesized aqua-based silver nanofluid from leaf extract in a helical double pipe heat exchanger: a comprehensive investigation[J].Journal of Thermal Analysis and Calorimetry,2024,149(7):2893-2905.
[15] Pang, L. P. Numerical Simulation of High - Temperature Ash Deposition on the Heating Surfaces of Power Station Boilers [J]. Proceedings of the CSEE, 2004(10): 219 - 223.
[16] Ye, J. M. Real - Time Monitoring System of Ash Deposition in Power Station Boilers Based on Kriging Model [J]. Boiler Technology, 2013, 44(6): 56 - 59.
[17] Zhang, H. L., Yang, S. R., Wang, S. L., et al. Thermal Percolation Model of the Effective Thermal Conductivity of the Ash Deposition Layer on the Tail Heating Surface of the Boiler [J]. Proceedings of the CSEE, 2005, 25(2): 135 - 138.
[18] Wang, B. Z. Feature Extraction of Slagging Faults on the Water - Wall of Pulverized Coal Furnaces [J]. Journal of Tsinghua University: Science and Technology, 1998(5): 64 - 68.
[19] Khairulmaini M ,Michael Z ,Hamid A F M , et al.Analyzing The Influence of Diameter and Winding on Heat Transfer Efficiency in Spiral Tube Heat Exchangers: A CAD-Integrated CFD Study Using Solidworks Flow Simulation[J].Journal of Physics: Conference Series,2024,2688(1).
[20] Chen, J. Z., Sun, X. Q., Lin, C. W., Jiang, Y., & Chen, S. H. Research on Intelligent Soot - Blowing Technology and Its Application in Ultra - Supercritical Boilers [J]. Power & Energy, 2020(02).
[21] Clay W, Davidson I S. Heat flux-meters in furnace boilers to monitor slag deposition[C]. Proc. Symp. on Thermal and Temperature Measurements in Science and Industry. IMECO Liverpool, 1987: 195-211
[22] Wei, J., Xiao, J. M., & Wang, T. Monitoring of Ash Fouling on the Heating Surfaces of 660 MW Boilers and Practical Application of Intelligent Soot - Blowing Systems [J]. Energy Research and Management, 2022(01): 87 - 92.
[23] B. H A ,Bilal M A ,Bilal M Q , et al.Numerical simulation of flow and heat transfer in a pipe with nail-shaped hurdles[J].Case Studies in Thermal Engineering,2024,53103906-.
[24] Zhou, J. B., Chen, X. W., Gao, H. D., Gao, L., Wang, L., Guo, Y. W., & Hou, Y. T. Monitoring of Ash Fouling on the Heating Surfaces of Coal - Fired Power Station Boilers and Intelligent Soot - Blowing Control Technology [J]. Thermal Power Generation, 2017(12).
[25] Hill D, KAINE P. Going for a clean sweep[J].Power engineering international,1998, 6(3):43-46